Impact evaluation of green-grey infrastructure interaction on built-space integrity: an emerging perspective to urban ecosystem service

Abhishek Tiwary[a, *]

[a]*Faculty of Engineering and the Environment, University of Southampton, Highfield, Southampton SO17 1BJ, United Kingdom.*

Email: a.tiwary@soton.ac.uk

Phone: +447866187059

Prashant Kumar[b, c]

[b]*Department of Civil and Environmental Engineering, Faculty of Engineering and Physical Sciences (FEPS), University of Surrey, Guildford GU2 7XH, United Kingdom.*

[c]*Environmental Flow (EnFlo) Research Centre, FEPS, University of Surrey, Guildford GU2 7XH, United Kingdom*

Email: p.kumar@surrey.ac.uk

Abstract

This paper evaluates the role of urban green infrastructure (GI) in maintaining integrity of built-space. The latter is considered as a lateral ecosystem function, worth including in future assessments of integrated ecosystem services. The basic tenet is that integrated green-grey infrastructures (GGIs) would have three influences on built-spaces: (i) reduced wind withering from flow deviation; (ii) reduced material corrosion/degeneration from pollution removal; and (iii) act as a biophysical buffer in altering the micro-climate. A case study is presented, combining the features of computational fluid dynamics (CFD) in micro environmental modelling with the emerging science on interactions of GGIs. The coupled seasonal dynamics of the above three effects are assessed for two building materials (limestone and steel) using the following three scenarios: (i) business as usual (BAU), (ii) summer (REGEN-S), and (iii) winter (REGEN-W).

Apparently, integrated ecosystem service from green-grey interaction, as scoped in this paper, has strong seasonal dependence. Compared to BAU our results suggest that REGEN-S leads to slight increment in limestone recession (<10%), mainly from exacerbation in ozone damage, while large reduction in steel recession (up to 37%) is observed. The selection of vegetation species, especially their bVOC emissions potential and seasonal foliage profile, appear to play vital role in determining the impact GI has on the integrity of the neighbouring built-up environment.

Keywords: Air Pollution; Building integrity; CFD; Dose-response function; Ecosystem service; Green infrastructure

---

Research Highlights: (3 to 5, each 85 characters including spacing)

- Green-grey interaction, i.e. impact of urban greening on built-up space is studied.
- A lateral ecosystem function of GI in built-space integrity is identified.
- Material surface recession for limestone and steel are computed under influence of GI.
- Material loss for steel is estimated to be over 5 times higher than for limestone.
- GI species selection and seasonal variation influence integrated ecosystem service.

1. Introduction

Incorporating green infrastructure (GI) into the urban built-space is gaining popularity as a cost-effective and long term measure for mitigating climate change impacts associated with proliferating grey infrastructure globally (CABE 2010; Hamdouch and Depret, 2010; Llausàs and Roe, 2012; MEA, 2005; Schäffler and Swilling, 2013; Thaiutsa et al., 2008). In essence, this is being achieved by utilising their ecosystem functions i.e. facilitating interactions between ecosystem structure and processes that underpin the capacity of an ecosystem to provide goods and services (Defra, 2011; TEEB, 2012). The UK National Ecosystem Assessment (NEA, 2011) have identified the following four broad categories of ecosystem services i.e. benefit people obtain directly or indirectly from ecosystems: (i) supporting (i.e. facilitating habitats for species); (ii) provisioning (i.e. generating resources); (iii) regulating (i.e. moderating climatic and biological effects), and (iv) cultural (i.e. recreational and aesthetic). Exploring the potentials of quantitative and qualitative approaches for assessing ecosystem services is a relatively new science, developing rapidly through a combination of numerical modelling and spatial analysis tools (Busch et al., 2012; Scholz and Uzomah, 2013). Among the regulating services of GI, the majority of efforts till date have been concentrated on assessing the direct benefits, for example, ecological and human health implications. The application of ecosystem service values to a new area such as built-space integrity is a novel contribution to knowledge and understanding. Such knowledge development is vital for fostering an inclusive green-grey urban (and landscape) planning, with the consideration for the 'extended ecosystem service' to facilitate sustainable urban futures.

Ample efforts have gone in determining the role of vegetation on urban microclimates, with numerous studies applying detailed physical as well as CFD simulations to assess the modifications to pollution concentrations through coupled effects of building morphology and vegetation on pollutants dispersion. These studies fall under two schools of thinking, depending on the building-vegetation biophysical interactions. One, projecting their positive influence by considering them as pollutant sinks (e.g., filtration and absorption of particulates and NO_x; Buccolieri et al. 2011; Tiwary et al., 2009, 2013a). Two, elucidating their negative influence as obstacles to airflow i.e. hampering the mixing of pollutants in poorly ventilated areas close to streets and reduced air exchange with the above-roof ambient environment (Gromke, 2011; Vos et al., 2012; Wania et al., 2012).

The majority of vegetation studies on buildings have focussed mainly on the assessment of thermal comfort (Ali-Toudert and Mayer, 2007; Berkovic et al., 2012; Berry et al., 2013; Santamouris, 2012; Yu and Hien, 2006) and reduced building energy demands (Akbari et al., 2001; Bouyer et al., 2011; Yang et al., 2012). A more recent study evaluated the role of urban green commons - comprising mainly of collectively managed parks, community gardens and allotment areas – in developing resilience and environmental stewardship in cities (Colding and Barthel, 2013). However, to our knowledge, no dedicated assessment of the impact of GI on the integrity of the surrounding 'grey infrastructure', including bridges, car parks and historical buildings, through their coupled aerodynamic and biophysical interactions have been conducted so far. Developing such understanding is pertinent to the on-going emphasis on enhancing GI investments as a tool in large scale climate change adaptation strategies. Moreover, this would aid holistic assessment of GIs by integrating all relevant sciences to sustain ecosystem services (Lundy and Wade, 2011; McMinn et al., 2010). The relevance of such study is greater now in the face of recent projections suggesting accentuations in the theoretical building dose-response functions (DRFs; the metrics commonly used to assess integrated exposure of building materials due to air pollutants and meteorological parameters.) under air pollution and changing environment, mainly owing to the altered micro-meteorological profile and chemical withering of building materials (including concrete, steel, stone, wood) under changing weather patterns (Brimblecombe and Grossi, 2008; Kumar and Imam, 2013). Such impacts need to be understood fairly swiftly, for both inner city and free-field environments, in the context of the modifications brought by the upcoming GI interventions.

The aim of this study is to enhance the understanding of the role of urban GI in ameliorating the micro-meteorological parameters and pollutant concentrations in an urban space, and the impact of these alterations on the material recession of surrounding built structures, such as building walls and bridges. Essentially, the modelling approach applied here is somewhat a hybrid assessment of what people have seen until now in individual pockets. The case study demonstrates the ecosystem services (or disservices) from GI in terms of their impact of built-space integrity, which has not been adequately accounted for in the conventional evaluation of their ecosystem functions so far. In particular, the following three influences of GI on the existing built-space are assessed: (i) as *quasi* bluff bodies in modifying the wind fields and withering; (ii) in reducing ambient pollution, and (iii) in altering the micro-climate. All these collectively influence the integrity of neighbouring built-spaces. The study

envisages promoting designing of cohesive green-grey infrastructures (GGIs) as future of sustainable city planning.

2. Methodology

2.1 Environmental modelling case study

The case study is designed to assess the role of GI for two contrasting seasonal conditions (summer and winter), typically representative of temperate climes. These were developed to understand the role of varying microclimatic effects from GI intervention on the integrity of 'inner-city' built infrastructure – both historical and new constructions. Keeping this in mind, the scenarios covered solid limestone wall structures (traditional buildings in European cities) and carbon steel structures (modern buildings). The domain comprised of a busy street canyon environment, exposed to traffic emissions, to ascertain the level of intervention offered by GIs in modifying the following two key factors influencing building integrity: (i) microclimate (wind, temperature, humidity), and (ii) pollutant profile (source/sink).

2.1.1 Base case

As a first step, a base case model was developed for business-as-usual (BAU) scenario. A fast response building-resolved Lagrangian dispersion modelling platform, QUIC - Quick Urban and Industrial Complex v5.81, with computational speeds and model complexities in between a Gaussian and a CFD model, was applied (Nelson and Brown, 2010). Its appropriateness for this task was ascertained based on its recent applications in urban flow simulations around built-up area (Hanna et al., 2011; Zwack et al., 2011). The modelling platform comprises of three sequential components – a city builder, a flow simulator (QUIC-URB or QUIC-CFD), and a dispersion calculator (QUIC-PLUME).

The QUIC model domain used a nested gridding with inner domain of 300m×300m×20m (length×breadth×height), mainly covering the 'grey' infrastructure (buildings, bridges and car parks) (shown in **Fig 1**). This was centred in an outer domain spanning 1000m×1000m×20m, allowing for evolution of the flow in the urban boundary layer to satisfy the guidelines for applications of CFD to simulate urban flows (Franke et al., 2007; Tominaga et al., 2008). The wind fields and pollutant dispersion for BAU were computed for a typical inner-city street environment, comprising of cross-streets lined with buildings, car parks (CP1, CP2) and

over-bridges (B1-B4) (**Fig. 1a**). The foot bridges (B1, B2) are located close to the cross-street intersection and the two cantilever car bridges (B3, B4) are located on approach to the two car parks, adhering to the design specification for over-bridges (DMRB, 2004). The meteorological inputs were acquired from a local weather station, including wind speed, ambient temperature, relative humidity, and ambient pressure.

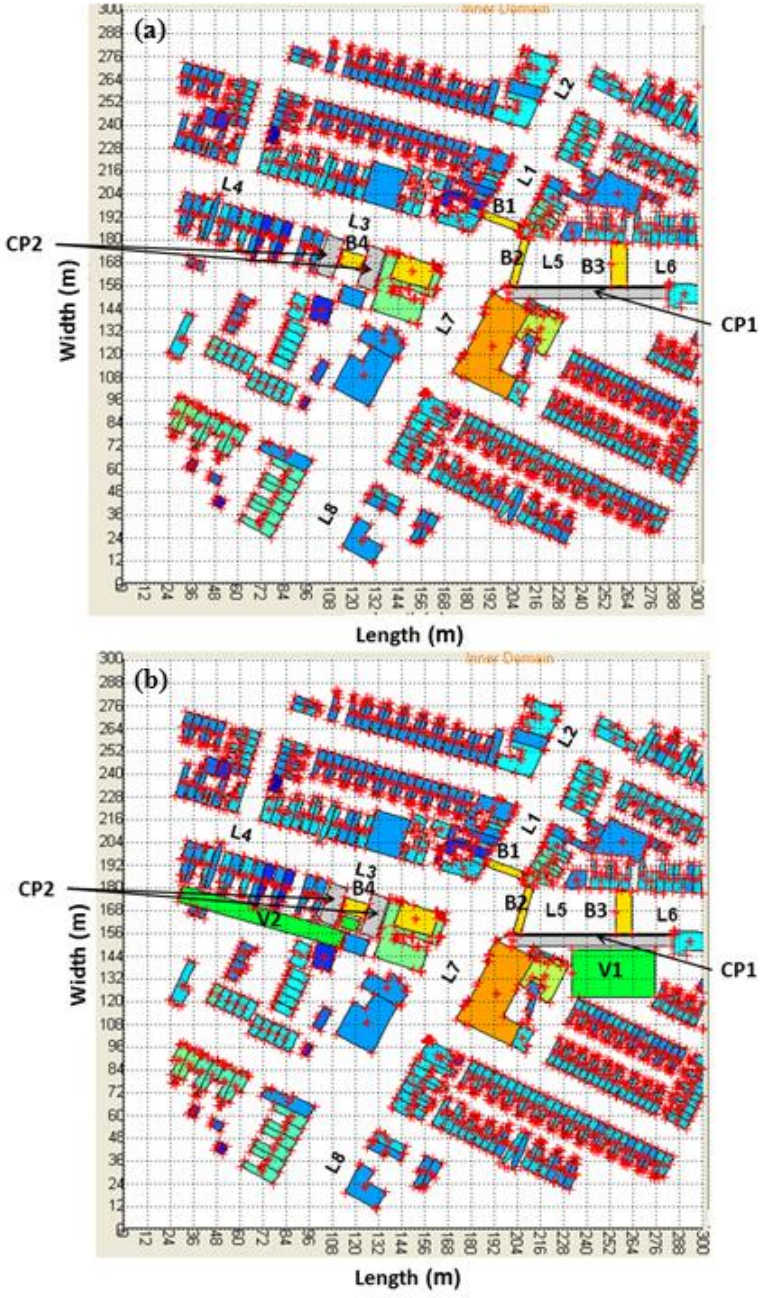

Fig. 1. Planar view of the model domain – (a) status quo (BAU, grey infrastructure only) with cross-streets showing location of foot bridges (B1, B2) and cantilever car bridges (B3, B4) across multi-storey car parks (CP1, CP2) respectively [note z=10m]; (b) Modified model domain for regenerated (REGEN, grey+green infrastructure) showing

the location of the proposed vegetation patches (V1, V2) [shaded green, includes a combination of shrubs and trees; buildings are colour-segregated on the basis of height].

As explained in **Section 2.1.2**, the wind direction was intentionally kept static at 210°. The road emissions were modelled as line sources for a typical European street environment (**Table 1**).

Table 1. Descriptors for road properties used in the BAU model set up as shown in planar view of Fig. 1a

Road Link ID	Width (m)	Link length (m)	Start coordinates*		End coordinates*		Building Height (m)	Direction (°N)
			North	East	North	East		
Link 1 (L1)	20	87.5	303563	457591	303465	457543	7	25
Link 2 (L2)	19	82.6	303620	457611	303672	457641	6	25
Link 3 (L3)	21	143.5	303470	457642	303465	457543	5	273
Link 4 (L4)	20	98	303509	457422	303541	457308	6	287
Link 5 (L5)	18	118	303492	457441	303465	457543	7	287
Link 6 (L6)	15	109	303445	457862	303455	457711	6	273
Link 7 (L7)	27	102.2	303352	457472	303465	457543	10	30
Link 8 (L8)	33	92.7	303283	457440	303352	457472	6	30

** UTMC Geo referencing coordinate system*

The simulation time period was set to allow the model to converge on a steady state solution. Pollutant concentrations for BAU were determined by quantifying the number of particles passing through a constant grid volume (5m×5m×2m) during the time period of interest. Concentrations were calculated on 1-min average basis in each grid volume. Pollutant concentrations were not calculated until the first released particles had passed completely over the domain and exited the downwind side (starting at 300 s). This step ensured the model computations to surpass evolutionary phase of the plume in order to output steady state concentration (Nelson and Brown, 2010). Overall, 766,500 'QUIC particles' were released over the entire 2000 s simulation.

2.1.2 Inclusion of Green Infrastructure

Two important considerations were made while introducing the GI for influencing both the microclimate and the resulting pollutant concentrations: (i) selection of vegetation species, and (ii) location of the plantations. Use of large urban trees has been recommended in the urban landscaping literature of the UK Construction Industry community to obtain higher

benefits (CIRIA, 2012). An earlier investigation reported net annual benefit of planting large tree species as 44% greater than for medium tree species and 92% greater than for a small tree species (McPherson et al., 1999). However, large trees in close vicinity of built structures tend to pose damage to the built environment due to vigorous root growth. In this study we applied the following combination of three vegetation species with distinct seasonal characteristics and vertical foliage profiles to test the dynamic role of vegetation buffers (their approximate area percentages provided alongside) – deciduous trees: Sycamore maple (*Acer pseudoplatanus* L.) (40%); deciduous hedgerow: Hawthorn hedge (*Crataegus monogyna*) (20%); coniferous tree: Douglas fir (*Pseudotsuga menziesii* (Mirb.) (40%). The hedgerows and trees were allocated uniform heights of 2m and 15m respectively, which is typical for inner city plantations in Europe. The idea was mainly to assess the microclimatic and pollution source/sink effects of deciduous species (Sycamore and Hawthorn) with negligible foliage in winter month to ascertain the holistic evaluation of GI effects. Our species selection corroborates with a recent tree survey, reporting Sycamore maple as the most abundant tree species in temperate and oceanic climate (typically over 35% of the mix) (Scholz and Uzomah, 2013). Further, the opted combination has been applied to assess the role of new planting in PM_{10} capture and its human health benefits for London (Tiwary et al., 2009).

To simulate the regeneration scenarios (REGEN), the BAU model domain was modified to include two vegetation patches (V1 and V2), away from streets and in the available open spaces upwind of the two car parks CP1 and CP2 respectively (assuming the prevailing wind enters the model domain in the lower left corner) (**Fig. 1b**). V1 and V2 were modelled respectively as high and low density vegetation canopy buffer spaces, close to existing grey-infrastructure, using two different arrangements of hedges and trees, typical of urban GI and commonly found in temperate climes. While the area percentage of the three selected species for both V1 and V2 were kept similar, the species were grouped to test different configurations - V1 was composed of two rectangular blocks, comprising of conifers in the central part and surrounded by deciduous trees and hedgerows in the outer ring. On the other hand, V2 was composed of a line of conifer trees giving a wind break effect, with a row of deciduous species (hedges and trees) located immediately upwind of CP2 (**Fig 2**).

Altogether two regeneration scenarios (summer, REGEN-S and winter, REGEN-W) were simulated using representative, and somewhat contrasting, meteorological and vegetation

parameters. The seasonal variations to input configurations were adequately parameterised – summer was characterised by denser foliage and mild meteorological conditions (low wind speed, high temperature, and low humidity); winter was characterised by lower foliage in the crown and the ground layers (**Fig 3**) and aggressive meteorological conditions (high wind speed, low temperature, high humidity) (**Table 2**). For the sake of generalisation, summer was considered as between April and September and winter as between October and March; the micrometeorological parameters for 2012 was applied to model the surface recession. This year was chosen since 2012 has been recorded as a wet year in the UK mainland, with nearly 800 mm rainfall in the midlands, the highest for the last 6 years (about 30% more than the average year) with high number of rain days.

The vegetation patches representing the GI in this study were introduced upwind of the buildings and bridges assessed and away from the street geometry (i.e. the pollutant source). Such practice follows recommendations from recent literature suggesting roadside urban vegetation to be accentuating the pollutant concentrations (mainly from localised sources, including traffic), owing to reduced ventilation and poor mixing of the pollutants (Buccolieri et al., 2011; Gromke and Ruck, 2009; Vos et al., 2012). This was ensured by keeping the wind direction static at 210°, which enabled the receptor locations (CP1, CP2, B3, B4) used to assess the vegetation effects to remain downwind of the vegetation patches (V1 and V2) over the entire model run.

Owing to the lack of an all-inclusive vegetation modelling tool, which can allow estimation of the required parameters for DRF calculations, inclusion of GI was evaluated in two steps. In the first step, the BAU set up in QUIC was modified using its vegetation modelling features (Pardyjak et al., 2009) to simulate the two REGEN scenarios, albeit with limited success since it does not allow for explicit resolution of individual vegetation components (e.g., leaves, stems) of canopies. These are parameterised in terms of their bulk attenuation coefficient (Nelson and Brown, 2010), which can be either chosen from a library of attenuation coefficients for a list of species ranging from orchards to single/mixed species forests (Cionco, 1978), or can be customised. Essentially, this is an extension of the windbreak model (Raupach et al., 2001), capable of simulating one-way interactions in terms of the bulk drag effects of vegetation as bluff bodies on the mean air flow and pollutant deposition. Due to underperformance of almost 40-50% of the deciduous species included in the vegetation buffers in winter, the corresponding attenuation coefficients for winter period

were kept effectively 40% lower than that of the summer months (QUIC library value of 4.03 for maple-fir stand in REGEN-S and 2.42 for only fir stand in REGEN-W were used).

The QUIC model allowed evaluation of only two of the three vegetation effects on buildings scoped within this study – one, bluff-body effect, and the other, pollution reduction potential. It does not have any mechanism to simulate the dynamic biophysical interactions between the vegetation components and the built-structure. Therefore, in the next step, a 3D prognostic microclimate model, coupling the principles of computational fluid dynamics and thermodynamics (ENVI-met®; Bruse, 2013), was applied to evaluate the alteration in the local microenvironment from inclusion of GI. Its capabilities of modelling plant-atmosphere interactions in city environments, simulating aerodynamics, thermodynamics and the radiation balance in complex urban structures have been established through several studies (Bruse and Fleer 1998; Peng and Elwan 2012; Rosheidat et al., 2008; Spangenberg et al., 2008; Vos et al, 2012; Wania et al., 2012). The model implements computational schemes of a conventional CFD model into a detailed vegetation canopy module to capture the two-way interactions of local vegetation on the wind field and micro-climate - both the forward effect on the wind-field and the thermodynamic feedbacks of the vegetation on the ambient air according to position of the sun, urban geometry, vegetation, soils and various construction materials - by solving thermodynamic and plant physiological equations. This enabled more realistic description of the exchange processes between the built- and the green-infrastructure. Appropriate to the need of our application, the numerical schemes further incorporate these feedbacks while simulating the diffusion and deposition of pollutants (Steyn and Rao, 2010).

One limitation faced was that ENVI-met is designed for micro scale modelling so only a sub-set of the QUIC model domain, covering 110m×70m×20m, with a grid resolution of 5m×5m×2m was selected for the simulation of two-way exchanges. The latter grid cell size was chosen to make the computational steps consistent with the QUIC model simulation (see **Section 2.1.1**); typical resolutions available in ENVI-met range between 0.5m and 10.0m (Bruse, 2013). Further, to minimise the boundary effects, which may distort the output data, the model uses an area of nesting grids around the core of the model to move the model boundary away from the area of interest (Bruse, 2013). For this purpose, the central portion of the QUIC domain covering the main features of analysis, including vegetation patches (V1, V2) and the studied receptors location (CP1, CP2, B3, B4), were selected (**Fig. 2)**.

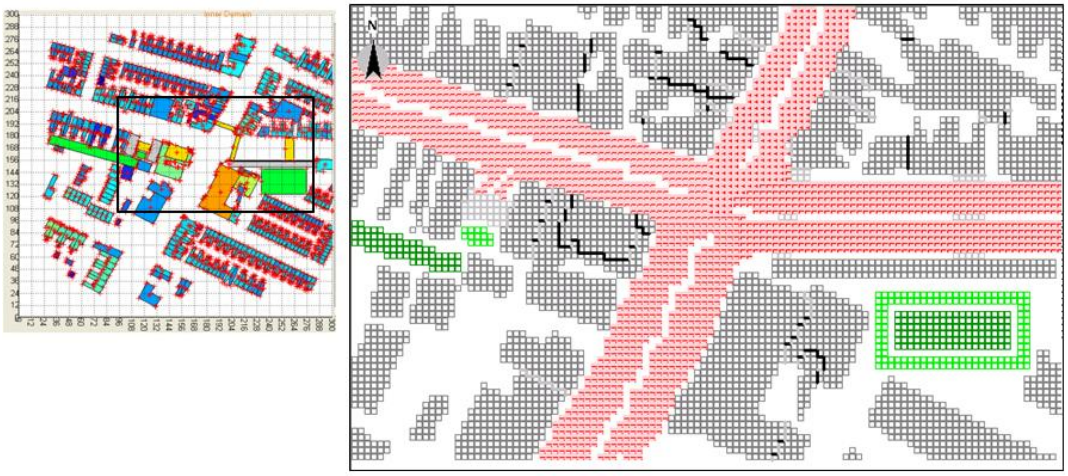

Fig. 2. ENVI-met simulation domain. The left panel shows portion of the QUIC model domain used for extended modelling in ENVI-met in the inset. (Gridded red mesh, separated by white space, represents two-lane traffic on each road; different shades of green mesh represent vegetation patches: Light green – Deciduous species; Dark green – Conifer species).

Following the QUIC approach, the traffic emissions in ENVI-met were modelled as cumulative line source emissions per lane. Representative foliage profiles for V1 and V2 were provided using the generic parameters in the plant database for hedge (2m) and trees (15m). The corresponding leaf area density (LAD) (m^2/m^3) profiles for the three vegetation species for the two seasons, applied to the 10 layers in the ENVI-met plan model (layer depth, Δz = 2m), are shown in **Fig. 3**. The maximum LAD for REGEN-S and REGEN-W is approximately 0.8 and 0.2 respectively (**Table 2**); the upright line in the lower most layer of REGEN-S at LAD = 0.8 represents the uniform deciduous hedgerow. It is noteworthy that the species composition (i.e. area percentages of the three species) of V1 and V2 are kept uniform over the two seasons and the only difference is in the spatial distribution of the LADs due to foliage loss in winter (as shown later in Fig 4). This is meant for evaluating the altered effects (if any) of the reduced GI intervention in REGEN-W. The local meteorological variables applied to the base case model were obtained from a weather station in Leicester and the upper air radiosonde data, accessed from the homepage of University of Wyoming (UWYO, 2013), for the closest sounding station at Watnall near Nottingham (station reference number: 03354; Latitude: 53°; Longitude: –1.25°; Altitude above mean sea level: 117 m; ~30 miles from the study site). Representative summer and winter scenarios were run as simulations for an entire day starting from daylight hours (24hr from 0600hrs GMT).

Table 2. Initial configuration data applied in the ENVI-met model scenarios.

	BAU (summer '12)	REGEN-S (summer '12)	REGEN-W (winter '12)
Atmosphere			
Simulation date/time range (GMT)	09 Aug 2012 (0600-2400 h)	09 Aug 2012 (0600-2400 h)	01 Jan 2012 (0600-2400 h)
Wind speed at reference height (10m above ground) [m s^{-1}]	5.2	5.2	3.7
Wind direction (degrees)	210	210	210
Initial air temperature [° K]	283	283	270
Relative humidity at 2m [%]	78	78	94
Specific humidity at 2500 m [g Water/kg air]*	5.5	5.5	7.9
Perceptible water [mm]	5.2	5.2	20.6
Buildings			
Albedo of walls	0.4	0.4	0.4
Albedo of roofs	0.3	0.3	0.3
Vegetation (see Figure 3)			
Maximum leaf area density (LAD) [m^2 m^{-3}]	N/A	0.8	0.2
Tree crown [m]	N/A	15	15
Shrubs/ Hedge [m]	N/A	2	2

** Source: University of Wyoming (UWYO, 2013)*

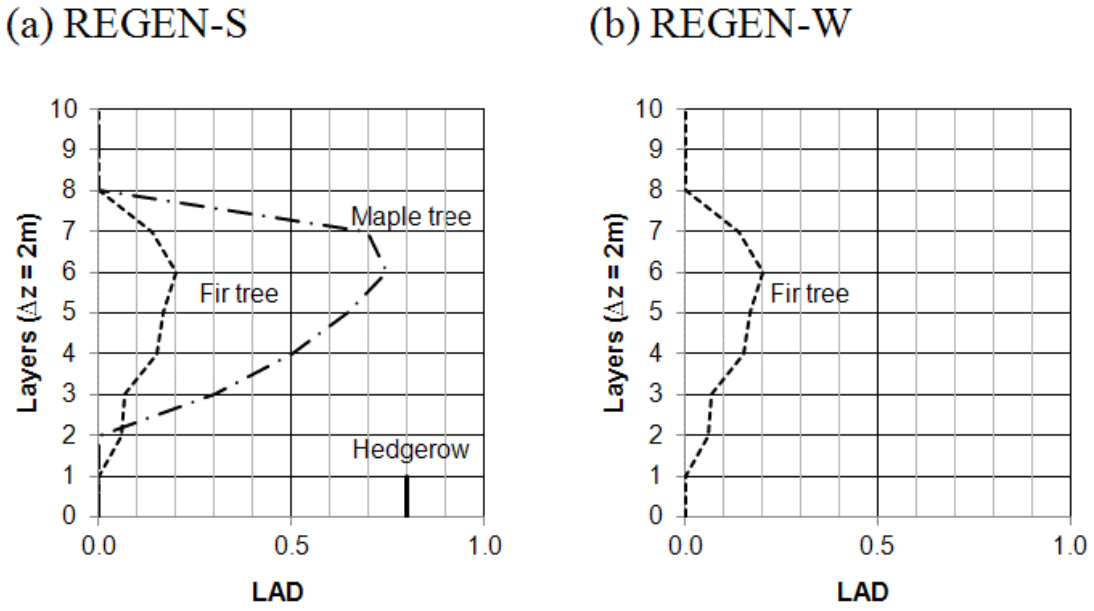

Fig. 3. Leaf Area Density profiles (LAD; m^2/m^3) for the three vegetation species (maple, fir and hawthorn) used in 10 layers of ENVI-met model for the two scenarios: (a) REGEN-S, (b) REGEN-W.

2.2 Building dose-response evaluation

Two different building materials – limestone and carbon steel – widely used in Europe, have been considered for the evaluation of material recession in unsheltered environmental conditions for the three scenarios (BAU, REGEN-S and REGEN-W). Evaluation of the impact of multi pollutants and meteorological conditions on built-space was assessed using the DRFs approach. The DRFs serve as a tool for assessing the material recession rate as a consequence integrated exposure of building materials to air pollutants (mainly NO_2, SO_2, PM_{10}, O_3 and CO_2) and meteorological parameters (primarily ambient temperature, relative humidity, wind field, pH). A number of DRF models are available in the published literature and the ones selected for our estimates, as summarised in a recent review article by Kumar and Imam (2013), are listed in appendix **Table A.1** (appendix). The choice of using more than one model is for comprehensiveness, essentially to capture the range of variation in the estimates. For instance, four type of DRF models are used for estimating the recession rate of limestone, developed by Lipfert (1989), Tidblad et al. (2001), Kucera et al. (2007) and Screpanti and De Marco (2009). Likewise, carbon steel DRFs are used, which were developed by Kucera et al. (2007) and Noah's Ark (2006).

In our study the driving parameters for DRF evaluation affected by GI interventions at the four earmarked receptor locations include pollutant concentrations (NO_2, SO_2, PM_{10}, O_3) and prevalent meteorology (ambient temperature, humidity, wind field). These were obtained for each of the three scenarios from the micro-environmental modelling steps; air temperatures were rounded off to the nearest whole number (**Table 3**). Dry deposition velocities for HNO_3 are based on the values reported in the literature and assumed to be 0.38 and 0.32 cm s^{-1} respectively (Kumar and Imam, 2013; Sabboni et al., 2006). A uniform CO_2 concentration was applied to the DRF assessments (383 ppm) for all four receptor locations. This can be argued to be acceptable since our aim was to analyse the relative effect of pollutant concentrations on structural material in the presence of vegetation. CO_2, largely being inert and abundantly available, is expected to remain spatially uniform for the four receptor sites. Likewise, the pH was also assumed to remain uniform as 5.2; representative Lipfert value of 18.8 was applied to the estimation following Brimblecombe and Grossi (2008). The maritime influence on the karst effect was ignored, given the study site was located away from sea in the midlands. Likewise, the estimates were made for ‘clean precipitation’, given that

deposition of sea salt aerosol has maximum effect within the first 100 m (Bonazza et al., 2009), which was considered negligible for the case study site in the UK midlands.

Table 3. Microclimate and pollutant concentrations (hourly average) at different receptor locations for the three scenarios modelled [Note: Reference height= 10m; Geo-reference origin (UTMX, UTMY): 457350m, 3033000m; Relative coordinates of receptors (+x, +y): CP1(252, 148), CP2(123, 160), B1(198, 188), B3(253, 168)].

	BAU	**REGEN-S**	**REGEN-W**
Annual Rainfall [mm]	602	602	962
Air Temperature* [°K]			
CP1	285	279	273
CP2	285	281	274
B1	285	285	272
B3	285	282	272
Relative Humidity* [%]			
CP1	72	80	89
CP2	72	78	95
B1	72	72	83
B3	72	75	87
Wind speed* [m s^{-1}]			
CP1	4.6	1.0	1.3
CP2	4.6	2.4	1.9
B1	4.8	4.3	2.6
B3	4.7	2.4	1.3
NO_2 [$g.m^{-3}$]*,a,†			
CP1	6.98E-05	6.77E-05	8.17E-05
CP2	3.09E-05	3.00E-05	3.37E-05
B1	1.64E-04	1.55E-04	2.21E-04
B3	1.19E-04	1.12E-04	1.97E-04
SO_2 [$g.m^{-3}$]#,b			
CP1	3.87E-06	3.79E-06	5.26E-06
CP2	3.20E-06	3.14E-06	4.15E-06
B1	4.78E-06	4.73E-06	7.33E-06
B3	4.23E-06	4.21E-06	5.47E-06
PM_{10} [$g.m^{-3}$]#,a,†			
CP1	1.83E-05	1.65E-05	1.91E-05
CP2	1.67E-05	1.46E-05	1.85E-05

B1	1.90E-05	1.73E-05	2.02E-05
B3	1.63E-05	1.47E-05	1.76E-05
O_3 [$g.m^{-3}$]^{*,b,†}			
CP1	8.24E-05	9.06E-05	3.37E-05
CP2	6.87E-05	7.26E-05	2.42E-05
B1	7.02E-05	7.72E-05	1.64E-05
B3	6.44E-05	7.08E-05	1.17E-05

CP = Car park; B =Bridge
$^{\#}$ *from QUIC*
* *from ENVI-met*
^{a} *only traffic source*
^{b} *traffic + urban background*
† *accounts for additional sources/sinks under vegetation effects during summer for O_3, NO_2 (Tiwary et al, 2013) and PM_{10} (McDonald et al., 2007).*

It is worth noting that extensive model validation (i.e. cross-comparison) exercise was not scoped within this study, mainly owing to the complexities in setting up a dedicated field measurement campaign (or a wind tunnel experiment) for validating the modelled parameters alongside. The model scenarios were developed using a set of static vegetation and meteorological parameters, without inclusion of all possible uncertainties therein. This begs a level of prudence while interpreting the results in the following sections as absolute values, accommodating for the uncertainties likely to propagate from individual modelling stages into the final outcome. While we have incorporated the level of variations in the predictions of vegetation effects on building integrity from different DRF models for the two seasons (as error bars in **Fig. 5**), our results should be considered only as overall estimates of the impacts such interactions may have to highlight the need for their inclusion in future integrated ecosystem assessments.

3. Results and Discussions

3.1. Evaluation of environmental parameters

A comparison table has been generated (**Table 3**) for the modelled micro-environmental parameters (air temperature, relative humidity, wind speed) and pollutant concentrations (NO_2, SO_2, PM_{10}, O_3) output at four strategically selected receptor locations – two car parks (CP1, CP2) and two bridges (B1, B3) (see **Fig. 1** for spatial references of these receptors). CP1 and CP2 were considered suitable as the two built structures immediately downwind of the high density and the low density vegetation patches (V1 and V2, respectively); B1 represented a cross-street location downwind and away from trees (i.e. unperturbed site); B3

represented a deeper canyon location in side street L5, downwind of car park CP1. For all these receptor locations the simulation outputs were obtained for the three modelled scenarios (BAU, REGEN-S and REGEN-W). It is noteworthy that BAU can only be directly compared with REGEN-S owing to similarity in underlying meteorology, whereas REGEN-W had inherently dominant winter characteristics in both foliage profile and meteorology. This pattern of model comparison is adopted hereafter throughout the discussion.

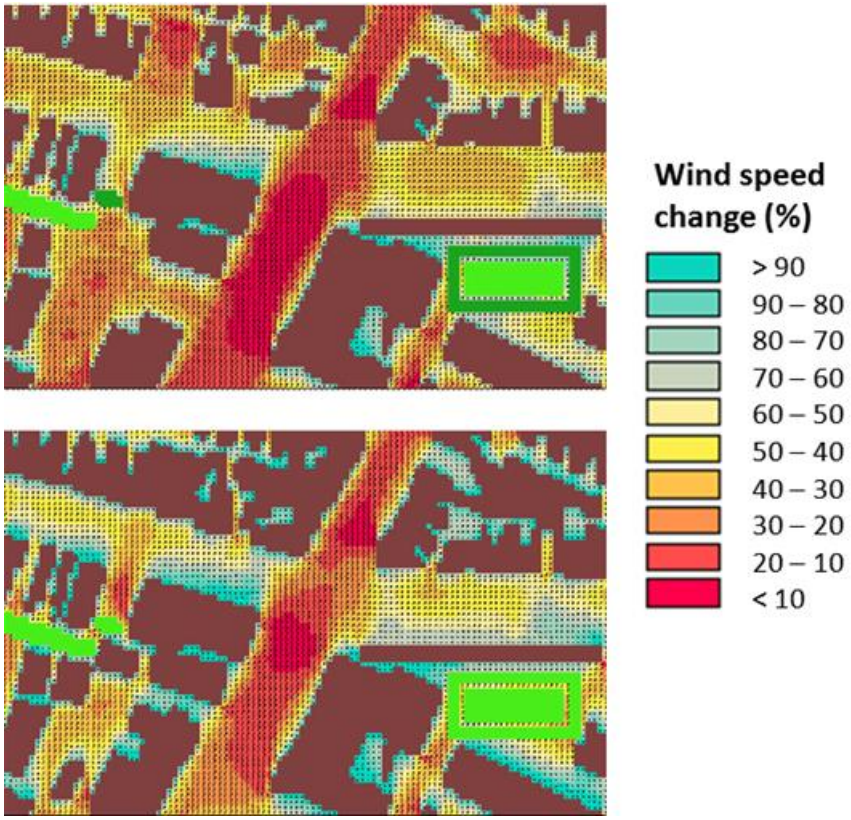

Fig. 4. Spatial plot of regeneration scenarios for wind speed change (%) output showing the seasonal dependence on meteorological and vegetation effect. Upper panel –summer (REGEN-S); Lower panel - winter (REGEN-W). (Darker green vegetation (both V1 and V2) in REGEN-S represents additional deciduous foliage, leading to higher effective LAD).

Preliminary results from this assessment indicate inclusion of GI to be largely affecting humidity and wind fields, with only marginal influence on the ambient air temperature. Compared to BAU the relative humidity downwind of dense vegetation (V1) is found to be about 10% higher for REGEN-S and the corresponding value is about 20% higher for REGEN-W. Overall, REGEN-S showed lowering while REGEN-W shows slight increment of air temperature at CP1 and CP2 compared to B1; the relative reductions being nearly two-

folds higher closer to high density patch (V1) compared to low density patch (V2). This is attributable to the fact that vegetation can lower the temperature of the air and can increase the humidity of the air during hot summer. These observations are consistent with previous studies (Spangenberg et al., 2008; Yang et al., 2012), suggesting the cooling effects of urban vegetation. However, the reported trends are based on pure modelling exercise, which is subjected to numerous uncertainties - both during evaluation of the individual parameters and from their application in the model formulations. As a consequence, these estimates should only be treated as a pathway towards developing any strategic implementation plan for future GIs. Nonetheless, we demonstrated successful implementation of this tiered modelling approach in assessing the impacts of urban green on built-up environment, giving some vital insights into the green-grey interactions in the inner city environment.

For REGEN-W, regions with high density patch (V1) and low density patch (V2) were respectively 1.1°C and 0.8°C (i.e. slightly higher air temperature than BAU). Such warming, instead of cooling in sub-zero temperatures with low sunlight (hence reduced or negligible evapotranspirative cooling), is owing to the fact that shading and evaporative cooling effect of the vegetation is hugely reduced in winter, which is beneficial for buildings. This has also been observed in another study for winter air temperature simulations (Yang et al., 2012) and attributable mainly to the inactive evaporation from vegetation in low sunlight regime, augmented by the discounted contributions of lost foliage from deciduous trees in winter.

The second half of **Table 3** lists the concentration distribution for a number of regulated pollutants at the selected receptor locations which are considered crucial for estimation of surface recession of limestone and carbon steel (**Section 3.2**). A general spatial and seasonal pattern for pollutant distribution was noted for the chosen receptor locations. This essentially reflected the compounding effects of the underlying model mechanism, with strong association with proximity to the street geometry, meteorology and vegetation source/sink effects. For example, NO_2 concentrations at bridge locations, being closer to the road sources, were higher than off-road car park locations; B1 showed higher values than B3 because of being located downwind of the intersection. Although the SO_2 concentrations remained slightly higher close to road sources (B1, B3) compared to off-road sites (CP1, CP2); the SO_2 loadings were found to be fairly uniform, mainly owing to the fact that modern vehicles have marginal sulphur emissions. It is worth noting that the winter concentrations bear resembling distribution profile, except showing higher values across the whole model domain. This is

possibly due to the lowering of the boundary layer during colder months, leading to localised enhancement of pollution at these sites. The concentrations for REGEN-S were generally lower than for BAU for most of the pollutants accounting for the sink terms, except for ozone. Slight increments were observed for the latter, especially at off-street locations (CP1, CP2), possibly from enhanced ozone photochemistry in presence of bVOC active broad-leaved maple during the summer. However, for REGEN-W the corresponding concentrations were much lower compared to BAU, which could be due to lack of precursor bVOCs and low solar radiation.

3.2 Evaluation of building integrity

Utilising the micro-environmental parameters obtained from previous steps, the building integrity was evaluated in terms of surface material recession based on DRF. As described in S**ection 2.2** this exercise was limited to limestone and carbon steel in the study, restricted by the availability of dose-response formulations for these two materials extensively in the literature. The resulting surface recession estimates at the four receptor locations CP1, CP2, B1 and B3 for these two materials are compared from the available models in **Figs. A.1 and A.2,** respectively (see appendix). The surface recession is estimated in terms of depth of material loss (µm) in a year. These can be converted to annual mass of material loss per unit area (g m^{-2}) by multiplying the material surface recession (µm yr^{-1}) with the density of carbon steel (~7850 kg m^{-3}) or lime stone (~2160 kg m^{-3}; for type II medium density). For example, this approach gives ~106.23 and 18.95 g of material loss per m^2 area per year for 13.52 and 8.77 µm yr^{-1} of surface recession in BAU (CP1) for carbon steel and lime stone, respectively. Surface recession (µm yr^{-1}) in this particular case is ~1.54 times higher for carbon steel compared with lime stone, but mass of material loss comes out ~5.60 times higher for carbon steel than those for lime stone, because of much higher density of the former material. The approximation of the material loss can be made accordingly for values presented for other scenarios in **Fig. 5**.

It is obvious from these figures that different DRF models provide variable results, which can be explained by the sensitivity of these models towards the various pollutants. In these models SO_2, NO_2, and O_3 are considered as important corrosive gases; SO_2 maintains a non-linear relationship with corrosion and its corrosive effect is maximum at a temperature of about 9–11 °C (Kucera et al., 2007). However, given the emission source were restricted to urban traffic SO_2 is not found to be a dominant pollutant in our case which leaves NO_2 and

O_3 as major contributors to the recession rates. Based on the model parameterisation (**Table A.1)** the DRF estimates for surface recession are found to be influenced in the following order by the underlying factors considered in this study (see **Table 3**): Limestone – Rain>>NO_2>O_3>SO_2>PM_{10}. Carbon Steel – Air temperature> SO_2>PM_{10}. Relative humidity has similar implications for all the materials and scenarios included in the study. Broadly, the models for limestone are based on the Lipfert function approach which has greater sensitivity to precipitation/rain (typical Lipfert function value used is 18.8×Rain). This dominates the whole surface recession estimates for limestone as clearly noted in **Fig. A.1**. On the other hand, carbon steel has not got NO_2 and O_3 effect, not because these do not affect it, but because these are not part of available DRFs. The surface recession estimates for steel is more sensitive to corrosive effects of pollutants (peaking at air temperature of about 282–284 °K) and therefore show much wider spatial variation for all the DRF models included in this assessment (**Fig. A.2**).

To show the relative changes from GI interventions, the surface recession estimates for limestone and carbon steel at the four receptor locations have been obtained as average from all available models (**Fig. 5**). Shown alongside in the same plots are the standard deviations, demonstrating the level of variations in the predictions from different models. For consistency, the observed values have to be compared separately in two sets, as follows - BAU is compared with REGEN-S as they are both using summer conditions (except the latter scenario incorporates additional biophysical effects of the introduced vegetation on the microenvironment and pollutant source/sink); REGEN-S is compared with REGEN-W to evaluate the seasonal dynamics in surface recession estimates, including the relative changes arising from the coupled vegetation-microenvironment effects (specifically the influence of reduced foliage from leaf shedding by deciduous species – maple and hawthorn) as well as the influence of the altered boundary layer on pollutant concentrations in sub-zero temperatures. The two sites immediately downwind of the vegetation patches (CP1 and CP2) show more prominent influences (Limestone – up to 10% increase; Steel – 28-37% decrease), whereas the site away from the vegetation patch (B1) has only marginal influence (Limestone – <2% increase; Steel – up to 7% decrease). It is noteworthy that the effects observed at B1 for steel in REGEN-W is arising from ambient wind conditions, away from vegetation effects (i.e. unperturbed site), which is much higher in winter (see Table 3). The observed increase for limestone surface recession in the presence of vegetation is attributed to slight enhancement in ground level ozone from introduction of bVOC active vegetation in REGEN-

S. This demonstrates the importance of species selection in optimising the ecosystem functions of GI on limestone buildings by avoiding exacerbation of ground level ozone during summer. On the other hand, steel is found to have greater reduction in surface recession estimates through GI intervention in summer, primarily owing to its independence from ozone damage.

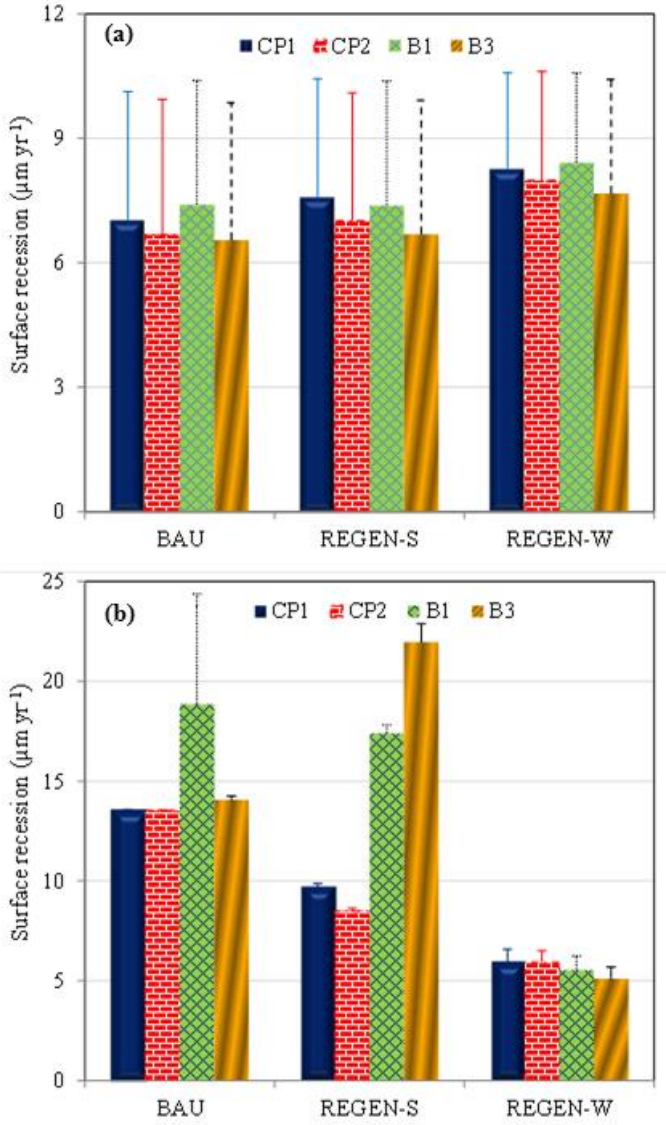

Fig. 5. Average recession of (a) lime stone and (b) carbon steel for all the three scenarios [note: only positive values of standard deviation are added for the clarity of figures].

However, some caution is required while interpreting the trends observed in Fig 5 as apart from vegetation effects there are additional influences incorporated in the model arising purely as artefacts of contrasting meteorological parameters between REGEN-S (which is same as BAU) and REGEN-W, which cannot be associated with vegetation as such. For example, evaluation of the seasonal effects alongside GI intervention show reverse effects on

surface recession values for limestone and carbon steel at B3 over the two contrasting seasons, which can be explained using the model parameters presented in Table 3 (much lower air temperature in winter months compared to BAU). Further, for limestone the average values at all the four receptors are slightly higher during winter (i.e. REGEN-W > REGEN-S) (**Fig. 5a**) whereas for carbon steel the corresponding values are much lower during winter (**Fig. 5b**). This is an interesting observation, useful to both research and planning communities, to take into account the varying seasonal influence of GI on different building materials. The observed winter enhancement of limestone material recession is primarily owing to heavier rain over the winter months compared to the summer months during the simulation period (see **Table 2**) combined with two-fold effects on exacerbation of ground level pollutant concentrations – one, due to loss of the vegetation sink from foliage loss by deciduous trees and hedges; two; from lowering of the atmospheric boundary layer in sub-zero temperatures (see **Table 3**). On the other hand, the observed summer enhancement of steel recession is primarily attributed to favourable temperature range of 282-284 °K, maximising the corrosive effects of acidic pollutants.

Apparently, due to the high density of built-up areas in the core model domain (about 82% including roads, bridges and buildings; **Fig. 1**), the overall surface recession reduction from the two vegetation patches (V1 and V2) is not substantial, albeit indicative of the potential for additional influence such intervention would hold for integrated green-grey infrastructure planning at the city-region levels. While our study mainly focussed on evaluating the role of different species on the basis of seasonal parameterisation of LAD, it revealed some inherent characteristics of GI which are strongly dependent on their species composition, including inhibition of particulate sink over winter, enhancement of ozone formation potential and wind speed reduction over summer. This is going to be enhanced further on the basis of appropriate vegetation selection, mainly the mix of evergreens with deciduous species to compensate for the seasonal effects in the face of climate change – catering to both warmer summers and harsher winters. Weighing all the negative and positive influences of GI (both existing and planned) in the urban ecosystem against each other is near-impossible and, as we showed through this example of estimating building integrity, is heavily marred by non-availability of all-inclusive model formulations. The thrust of the majority of such evaluations is currently on improving air quality and/or thermal comfort, and conservation of building surfaces, as highlighted through this study, is very much an emerging perspective of green-grey interactions (which is envisaged to get more intense with further increase in GGIs). However,

it is recommended that these findings be used only to get broader insight into this integrated urban ecosystem service; further scrutiny of detailed evaluation should take into account the uncertainty aspect of these interactions.

4. Conclusions

This study evaluated the role of modified urban microenvironment through inclusion of GI on building integrity; the metrics adopted is material surface recession of limestone and carbon steel. The dynamic seasonal characteristics in meteorology and foliage profile (for 60% deciduous component in the simulated vegetation) have been incorporated through two case study scenarios (for summer and winter) to portray the varying degrees of impacts over a year. The assessment has been conducted in two stages – first, utilising CFD modelling capabilities to quantify the aerodynamic features and bio-physical interactions between the grey and the green components of the city. In the next step, adequate model parameterisation from available literature was applied to estimate the coupled effects of pollutants and micro environmental variables on building material recession.

Our findings show the influence of GI on built-space integrity in terms of differentiating the four receptor locations used in the assessment. For example, the two sites immediately downwind of the vegetation patches (CP1 and CP2) show prominent changes in the summer scenario with GI intervention, REGEN-S compared to the BAU scenario. However, contrasting seasonal influences of GI on the surface recession rates of the two building materials have been noted. Slight increment in the surface recession is observed for limestone during winter whereas large reductions are found in recession of carbon steel during summer. This is quite revealing, as most GI assessments till date would assume only the positive influences of vegetation as windbreak and pollution sink, overlooking their pollution source contributions in affecting neighbouring built-space. The latter gains relevance in our study since both Sycamore maple and Douglas fir (making up to 80% of the vegetation buffer in our case study) are active sources of bVOC emissions over summer months. Given limestone recession is strongly influenced by ground-level ozone, availability of ozone precursors (through photochemical interactions of bVOC emissions with NO_2 from traffic) explain the observed increment. Hence, our integrated assessment of GI intervention on built-space integrity (**Fig. 5**) has shed light on their varying, and apparently reciprocal effects on the two building materials, primarily influenced by the bio-physical characteristics of the constituent

vegetation species and meteorological factors. The former gains relevance in summer months in terms of the enhanced bVOC emissions, serving as ozone precursor (a major contributor to surface recession for limestone). The latter gains relevance in winter months in exacerbating pollutant concentrations under harsher meteorology in temperate climes (primarily owing to lowering of the atmospheric boundary layer during the colder months). Whilst our modelling exercise provides broader insight and overall estimates of the interactions between the green-grey infrastructure and integrity of built-up space, studies focusing on detailed model validation exercises are needed for accurate estimations and for reducing the levels of uncertainty in the results.

Our study has shown the relevance of GI for future sustainability of green-grey infrastructure. We encapsulated the plausibility of a lateral ecosystem function of GI in built-space integrity, beyond the direct human benefits identified under the 'regulating' services of GI under the generic ecosystem service variable – local climate and air quality regulation (LCAR; LCAR accounts for the effects of trees and other plants in lowering the temperature by providing shade and influence water availability (e.g., evapotranspiration); regulating air quality by removing pollutants from the atmosphere (e.g., filtration and absorption of particulates and NO_x)). As a natural next step, this would warrant quantification of the lateral ecosystem functions offered by these initiatives in future urban environments, which are currently not taken into account as part of ecosystem service (NEA, 2011). Our results also highlight some of the challenges faced in spatial modelling of ecosystem services. More research is therefore recommended to develop the ecosystem service assessment approach further into a numerical model.

5. Acknowledgments

We acknowledge the technical assistance from Matt Nelson and Michael Brown at the Los Alamos National Laboratory, USA in setting up the QUIC model and from Prof. Michael Bruse, University of Mainz, Germany in setting up the ENVI-met model. Acknowledgments are also due to Peter Vos at Flemish Institute for Technological Research (VITO), Belgium in clarifying few issues in modelling the micro environmental feedbacks from vegetation intervention in built space using ENVI-met. We would also like to acknowledge the invaluable contributions from the anonymous reviewers towards further enhancement of this paper.

6. References

Akbari H, Pomerantz M, Taha H. Cool surfaces and shade trees to reduce energy use and improve air quality in urban areas. Solar Energy 2001;70:295-310.

Ali-Toudert F, Mayer H. Effects of asymmetry, galleries, overhanging façades and vegetation on thermal comfort in urban street canyons. Solar Energy 2007;81:742-54.

Berkovic S, Yezioro A, Bitan A. Study of thermal comfort in courtyards in a hot arid climate, Solar Energy 2012;86:1173-86.

Berry R, Livesley SJ, Aye L. Tree canopy shade impacts on solar irradiance received by building walls and their surface temperature, Building and Environment 2013;69:91-100.

Bonazza A, Messinaa P, Sabbionia C, Grossi CM, Brimblecombe P. Mapping the impact of climate change on surface recession of carbonate buildings in Europe. Sci. Total Environ 2009;407:2039-50.

Bouyer J, Inard C, Musy M. Microclimatic coupling as a solution to improve building energy simulation in an urban context, Energy and Buildings 2011;43:1549-59.

Brimblecombe P, Grossi C. Millennium-long recession of limestone facades in London. Environ. Geol. 2008; 56: 463-471.

Bruse, M., 2013. http://www.envi-met.com [accessed in Feb 2013].

Bruse M, Fleer H. Simulating surface–plant–air interactions inside urban environments with a three dimensional numerical model. Environ Model Softw 1998;13:373–84.

Buccolieri R, Salim SM, Leo LS, Di Sabatino S, Chan A, Ielpo P, de Gennaro G, Gromke C. Analysis of local scale tree-atmosphere interaction on pollutant concentration in idealized street canyons and application to a real urban junction. Atmos Environ 2011;45:1702-13.

Busch M, Notte AL, Laporte V, Erhard M. Potentials of quantitative and qualitative approaches to assessing ecosystem services. Ecol Indic 2012;21:89-103.

CABE. Urban Green Nation: Building the Evidence Base. UK Commission for Architecture and the Built Environment, London; 2010.

Cionco RM. Analysis of canopy index values for various canopy densities. B.-Layer Meteor. 1978;15:81-93.

CIRIA. The benefits of large species trees in urban landscapes: a costing, design and management guide. London: Construction Industry Research and Information Association; 2012.

Colding J, Barthel S. The potential of 'Urban Green Commons' in the resilience building of cities. Ecological Economics 2013;86:156-66.

Defra. Overarching impact assessment for the Natural Environment White Paper. UK Department of the Environment, Food and Rural Affairs London; 2011.
url-http://www.archive.defra.gov.uk/environment/natural/documents/newp-ia-110607
[accessed in Feb 2012].

DMRB. Design Manual of Roads and Bridges – Design Criteria for Footbridges; London; 2004. url-http://www.dft.gov.uk/ha/standards/dmrb/vol2/section2/bd2904.pdf
[accessed in Jul 2012].

Exposure Standards for Atmospheric Contaminants in the Occupational Environment—Guidance Note [NOHSC:3008(1995)].

Franke, J., Hellsten, A., Schlünzen, H., Carissimo, B., 2007. Best practice guideline for the CFD simulation of flows in the urban environment, COST Guidelines. Hamburg.

Gromke C. A vegetation modeling concept for building and environmental aerodynamics wind tunnel tests and its application in pollutant dispersion studies. Environ Pollut 2011;159:2094-99.

Gromke C, Ruck B. Effects of trees on the dilution of vehicle exhaust emissions in urban street canyons. Int J Environ Waste Manag 2009;4:225-42.

Hamdouch A., Depret M-H. Policy integration strategy and the development of the 'green economy': foundations and implementation patterns. J Environ Planning and Manag 2010;53(4):473–90.

Hanna S, White J, Trolier J et al. Comparisons of JU2003 observations with four diagnostic urban wind flow and Lagrangian particle dispersion models. Atmos Environ 2011;45:4073-81.

Kucera V, Tidblad J, Kreislova K, Knotkova D, Faller M, Reiss D, Snethlage R, Yates T, Henriksen J, Schreiner M, Melcher M,, Ferm M,, Lefèvre R-A, Kobus J. UN/ECE ICP Materials Dose-response Functions for the Multi-pollutant Situation. Water, Air & Soil Pollut: Focus 2007;7:249-58.

Kumar P, Imam B. Footprints of air pollution and changing environment on the sustainability of built infrastructure. Sci. Total Environ 2013;444:85-101.

Lipfert FW. Atmospheric damage to calcareous stones: Comparison and reconciliation of recent experimental findings. Atmos Environ (1967),1989;23:415-29.

Llausàs A, Roe M. Green Infrastructure Planning: Cross- National Analysis between the North East of England (UK) and Catalonia (Spain). European Planning Studies 2012;20(4):641-63.

Lundy L, Wade R. Integrating sciences to sustain urban ecosystem services. Prog Phys Geogr 2011;35:653–69.

McDonald AG, Bealey WJ, Fowler D, Dragosits U, Skiba U, Smith RI, Donovan RG, Brett HE, Hewitt, CN, Nemitz E. Quantifying the effect of urban tree planting on concentrations and depositions of PM10 in two urban conurbations. Atmos Environ 2007;41:8455-67.

McMinn WR, Yang Q, Scholz M. Classification and assessment of water bodies as adaptive structural measures for flood risk management planning. J Environ Manag 2010;91(9):1855–63.

McPherson EG, Simpson JR, Peper PJ, Qingfu X. Benefit-cost analysis of Modesto's municipal urban forests. J Aboric 1999;25(5):235–48.

MEA. Millennium Ecosystem Assessment: Ecosystems and human well-being. Washington: Island Press; 2005.

NEA. The UK National Ecosystem Assessment: Synthesis of the Key Findings. United Nations Environment Programme World Conservation Monitoring Centre. Cambridge Press; 2011.

Nelson M, Brown M. The QUIC Start Guide (V5.6), LA-UR-10-01062. Los Alamos National Laboratory; 2010.

Noah's Ark. Global climate change impact on built heritage and cultural landscapes. Overview of the expected negative and positive consequences of global environmental changes on deterioration of materials Project Report No. SPPI-CT-2003-501837-NOAH'S ARK; 2006.

Pardyjak E, Amatul UN, Nelson MA, Brown MJ. Development of a vegetation deposition model for a fast response urban Lagrangian dispersion model. Eighth Symposium on the Urban Environment. American Meteorological Society, Phoenix Arizona; 2009.

Peng C, Elwan FA. Bridging outdoor and indoor environmental simulation for assessing and aiding sustainable urban neighbourhood design. Int J Arch Res 2012;6:72-90.

Raupach MR,Woods N, Dorr G, Leys JF, Cleugh HA. The entrapment of particles by windbreaks. Atmos Environ 2001;35:3373–83.

Rosheidat A, Hoffman D, Bryan H. Visualising pedestrian comfort using ENVI-met. Third National Conference of IBPSA-USA, Berkeley, California, July 30 – August 1; 2008.

Sabboni C, Cassar M, Brimblecombe P, Tidblad J, Kozlowski R, Drdacky M, Saiz-Jimenez C, Grontoft T, Wainwright I, Arino X. Global climate change impact on building heritage and cultural landscapes. Heritage, Weathering and Conservation - Fort, Alvarez de Buergo, Gomez-Heras & Vazquez-Calvo (eds) ISBN 0-415-41272-2, 2006; 395-401.

Santamouris M. Cooling the cities – A review of reflective and green roof mitigation technologies to fight heat island and improve comfort in urban environments, Solar Energy 2012; http://dx.doi.org/10.1016/j.solener.2012.07.003.

Schäffler A, Swilling M. Valuing green infrastructure in an urban environment under pressure — The Johannesburg case, Ecolog Econ 2013;86: 246-57.

Scholz M, Uzomah VC. Rapid decision support tool based on novel ecosystem service variables for retrofitting of permeable pavement systems in the presence of trees. Sci Total Environ 2013:458-460:486-98.

Screpanti A, De Marco A. Corrosion on cultural heritage buildings in Italy: A role for ozone? Environ Pollut 2009;157:1513-20.

Spangenberg J, Shinzato P, Johansson E, Duarte D. Simulation of the influence of vegetation on microclimate and thermal comfort in the city of Sao Paulo. Rev. SBAU 2008;3:1-19.

Steyn DG, Rao ST (eds.) Air Pollution Modelling and Its Application, DOI 10.1007/978-90-481-3812-8, Springer Science, B.V; 2010.

TEEB. The Economics of Ecosystems and Biodiversity (TEEB) manual for cities: ecosystem services in urban management. The Ecological and Economic Foundation, chapter 1, p.19; 2012. url-http://www.teebweb.org [accessed in Oct 2012].

Thaiutsa B, Puangchit L, Kjelgren R, Arunpraparut W. Urban green space, street tree and heritage large tree assessment in Bangkok, Thailand. Urban Forestry & Urban Greening 2008;7:219-29.

Tidblad J, Kucera V, Mikhailov A, Henriksen J, Kreislova K, Yates T, Stöckle B, Schreiner M. UN ECE ICP Materials: Dose-Response Functions on Dry and Wet Acid Deposition Effects After 8 Years of Exposure. Water, Air, & Soil Pollution 2001;130:1457-62.

Tiwary A, Namdeo A, Fuentes J, Dore A, Hu X-M, Bell M. Systems scale assessment of the sustainability implications of emerging green initiatives, Environ Pollut 2013a;183:213-23.

Tiwary, A, Chatterton T, Namdeo A. Co-managing carbon and air quality: pros and cons of local sustainability initiatives. J Environ Planning Manag 2013b; doi:10.1080/09640568.2013.802677.

Tiwary A, Sinnett D, Peachey C, Chalabi Z, Vardoulakis S, Fletcher T, Leonardi G, Grundy C, Azapagic A, Hutchings T. An integrated tool to assess the role of new planting in PM10 capture and the human health benefits: a case study in London. Environ Pollut 2009;157:2645-53.

Tiwary A, Morvan HP, Colls JJ. Modelling the size-dependent collection efficiency of hedgerows for ambient aerosols. J Aerosol Sci 2006;37:990-1015.

Tominaga Y, Mochida A, Yoshie R, Kataoka H, Nozu T, Yoshikawa M, Shirasawa T. AIJ guidelines for practical applications of CFD to pedestrian wind environment around buildings. J Wind Engineering Ind Aerodnamics 2008;96;1749-61.

UWYO. Atmospheric Soundings. Department of Atmospheric Sciences, University of Wyoming, USA; 2013. url: http://weather.uwyo.edu/upperair/sounding.html. [accessed in March 2013].

Vos PEJ, Maiheu B, Vankerkom J, Janssen S. Improving local air quality in cities: To tree or not to tree?, Environ Pollut 2012;183:113-22.

Wania A, Bruse M, Blond N, Weber C. Analysing the influence of different street vegetation on traffic-induced particle dispersion using microscale simulations. J Environ Manag 2012; 94:91-101.

Yang X, Zhao L, Bruse M, Meng Q. An integrated simulation method for building energy performance assessment in urban environments, Energy and Buildings 2012;54:243-51.

Yu C, Hien WN. Thermal benefits of city parks. Energy and Buildings 2006;38:105-20.

Zwack LM, Hanna SR, Spengler JD, Levy JI. Using advanced dispersion models and mobile monitoring to characterise spatial patterns of ultrafine particles in an urban area. Atmos Environ 2011;45:4822-29.

Appendix

Table A.1. Summary of DRFs used for our estimates; table adopted from Kumar and Imam (2013). Please note that ML and R stand for mass loss by corrosion attack in g m^{-2} and surface recession or thickness loss in μm (>1–year exposure) or μm yr^{-1} (1–year exposure), respectively. Gaseous and ion concentrations are annual mean in μg m^{-3} and mg lit^{-1}. D_{cl} is chloride deposition (mg m^{-2} day^{-1}) and Rh_{60} = (Rh–60) when Rh >60; otherwise 0. Rn is precipitation in m yr^{-1}; V_{dS} and V_{dN} are deposition velocities (cm s^{-1}) for SO_2 and HNO_3, respectively.

Material	Dose–response function	Source
Carbon steel	$R = 1.58[SO_2]^{0.52} e^{[0.02Rh + fCs(T)]} + 0.166Rn[H^+] + 0.0761 PM_{10} + 0.102D_{Cl}^{0.33} e^{[0.033Rh + 0.040T]}$ $f_{Cs}(T) = 0.150(T–10)$ when $T \leqslant 10°C$ $f_{Cs}(T) = –0.054(T–10)$ when $T > 10°C$	Noah's Ark (2006)
	$R = 1.77[SO2]^{0.52} e^{[0.20Rh + fws(T)]} + g(Cl^–, Rh, T)$ $ML = 29.1 + t^{0.6} (21.7 + 1.39[SO_2]^{0.6} Rh_{60} e^{fWs(T)} + 1.29 Rn[H^+] + 0.593PM_{10})$ $f_{ws}(T) = 0.150(T–10)$ when $T \leqslant 10°C$ $f_{ws}(T) = –0.054(T–10)$ when $T > 10°C$	Kucera et al. (2007)
Portland limestone	$R = 2.7 [SO_2]^{0.48} e^{– 0.018T} t^{0.96} + 0.019 Rn[H^+] t^{0.96}$	Tidblad et al. (2001)
	$R = 3.1 + t(0.85 + 0.0059 Rh_{60} [SO_2] + 0.078 Rh_{60} [HNO_3] + 0.054Rn[H^+] + 0.0258 PM_{10})$ $[HNO_3] = 516 e^{–3400/(T+273)} ([NO_2][O_3] Rh)^{0.5}$	Kucera et al. (2007)
	$R = 18.8 Rn + 0.016 [H^+] Rn + 0.18 (V_{dS} [SO2] + V_{dN} [HNO_3])$	Lipfert (1989)
	[a]$R = 3.1 + t (0.85 + 0.0059[SO_2] Rh_{60} + 0.054 Rn[H^+] + 0.078 (516 e^{–3400/(T+273)} ([NO_2] [O_3] Rh)^{0.5} Rh_{60}) + 0.0258 PM_{10})$	Screpanti and De Marco (2009)

Nomenclature:
ML = Mass loss (g m^{-2})
R = Surface recession (μm yr^{-1})
SO_2 = Sulphur dioxide (μg m^{-3})
NO_2 = Nitrogen dioxide (μg m^{-3})
O_3 = Ozone (μg m^{-3})
PM_{10} = Particulate matter ≤10 μm in diameter (μg m^{-3})
T = Ambient temperature (°C)
t = time (years)
$f_{Cs}(T)$ = Correction factor depending on temperature (-)

$f_{ws}(T)$ = Correction factor depending on temperature (-)
Rh = Relative humidity (%)
V_{dS} = Deposition velocity of sulphur dioxide, SO_2 (cm s^{-1})
V_{dN} = Deposition velocity of nitric acid, HNO_3 (cm s^{-1})
D_{cl} = Chloride deposition (mg m^{-2} day^{-1})
Rn = Precipitation (m yr^{-1})

Fig. A.1

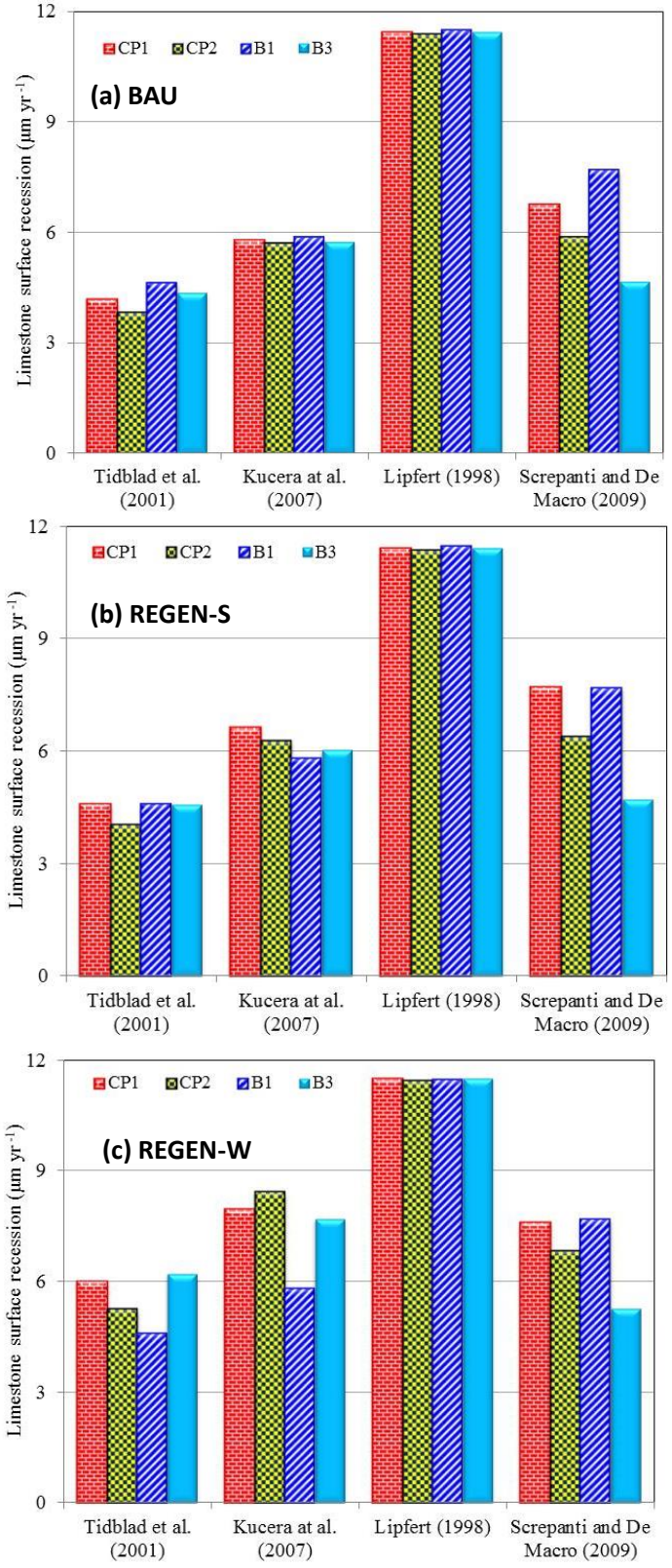

Fig. A.1. Recession of lime stone for all the three scenarios, using four different models.

Fig A.2

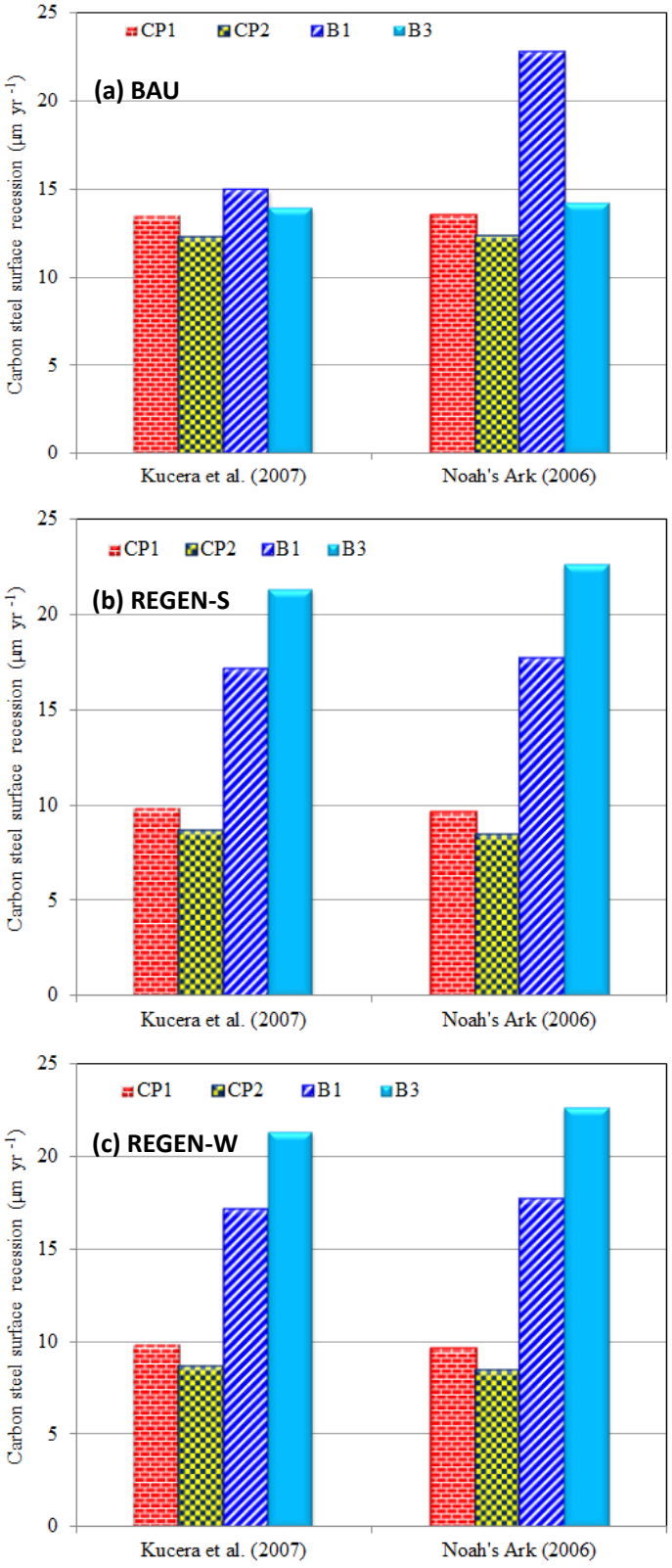

Fig. A.2. Recession of carbon steel for all the three scenarios, using two different models.